Micromodulating the Electronic Coupling Across Redox-Active Ferrocenyl Spacer in Binuclear Ruthenium(II) Terpyridine Complexes: Synthesis, Electrochemistry, and Photophysical Properties

Teng-Yuan Dong,*[,†] Hung-Yu Lin,[†] Shu-Fan Lin,[†] Chia-Chen Huang,[†] Yuh-Sheng Wen,[‡] and Liangshiu Lee[†]

Department of Chemistry, Center for Nanoscience and Nanotechnology, National Sun Yat-Sen University, Kaohsiung, Taiwan, and the Institute of Chemistry, Academia Sinica, Nankang, Taipei, Taiwan

Received June 11, 2007

The electrochemical and photophysical properties of $[(X\text{-tpy})Ru^{II}(tpy\text{-}(fc)_2\text{-}tpy)Ru^{II}(X\text{-tpy})]^{4+}$ (tpy = terpyridyl; X = −H (**1a**), $-OCH_3$ (**1b**), −Cl (**1c**); fc = ferrocenyl) and $[(X\text{-tpy})Ru^{II}(tpy\text{-}C{\equiv}C\text{-}(fc)_2\text{-}C{\equiv}C\text{-}tpy)Ru^{II}(X\text{-tpy})]^{4+}$ (X = −H (**2a**), $-OCH_3$ (**2b**), −Cl (**2c**)) are described. The ground-state HOMO and LUMO energies were probed by electrochemical measurements. The excited-state photophysical properties were probed by UV–vis absorption spectroscopy and luminescence spectroscopy. Complexes of **1a**−**c** are nonemissive (λ_{exc} 480–580 nm) in deoxygenated pure CH_3CN or H_2O/CH_3CN (4/1) solution at 25 °C. Complexes **2a**−**c** have room-temperature luminescence in H_2O/CH_3CN (4/1) solution. On comparison of the luminescent properties of **2b**,**c** with those of **2a**, the attachment of $-OCH_3$ and −Cl substitutents causes a decrease of luminescence quantum yields and triplet lifetimes.

Introduction

Over the past decade, the study of homo- and heterometallic binuclear transition-metal complexes in which the end-capped metal centers are connected by π-conjugated organic linear spacers has been an intriguing area of research, since such systems may provide the possibility of studying the electronic communication between the redox-active end-capped metal centers or serve as models for molecular wires.[1–3] In this context, end capping of unsaturated organic spacers with redox-active groups, such as ruthenium(II) polypyridine metal centers, have been mostly studied where they are intended to promote long-range electron or energy transfer.[4–6] The design of interesting bis(2,2′:6′,2″-terpyridine) ligands (tpy-tpy) by connecting two terpyridine moieties via a rigid organic spacer attached to their 4′-positions has found applications in energy conversion systems such as dye-sensitized solar cells[7] and electroluminescent devices.[8] Very recently, we have described the electrochemical and photophysical properties for a series of complexes containing redox-active bis(2,2′:6′,2″-terpyridyl)polyferrocenyl spacers end-capped with photoactive and redox-active Ru^{2+}−terpyridine terminals to study the electronic communication between the end-capped Ru^{2+} metal centers (Scheme 1; $[(tpy)Ru^{II}(tpy\text{-}(fc)_n\text{-}tpy)Ru^{II}(tpy)]^{4+}$ (fc = ferrocenyl, n = 1–3) and $[(tpy)Ru^{II}(tpy\text{-}C{\equiv}C\text{-}(fc)_n\text{-}C{\equiv}C\text{-}tpy)Ru^{II}(tpy)]^{4+}$ (n = 2, 3)).[9–12]

Our design principle for wirelike molecules is that the redox-active ferrocenyl spacer should enhance the capability of transfer information along the molecular axis. As shown in Figure 1, a large ground-state HOMO–LUMO energy gap (∼2.54 eV) in

* To whom correspondence should be addressed. E-mail: dty@mail.nsysu.edu.tw.

† National Sun Yat-Sen University.

‡ Academia Sinica.

(1) (a) Indelli, M. T.; Scandola, F.; Collin, J.-P.; Sauvage, J.-P.; Sour, A. *Inorg. Chem.* **1996**, *35*, 303–312. (b) Patoux, C.; Launay, J.-P.; Beley, M.; Chodorowski-Kimmes, S.; Collin, J.-P.; James, S.; Sauvage, J.-P. *J. Am. Chem. Soc.* **1998**, *120*, 3717–3725. (c) Beley, M.; Chodorowski-Kimmes, S.; Collin, J.-P.; Lainé, P.; Launay, J.-P.; Sauvage, J.-P. *Angew. Chem., Int. Ed. Engl.* **1994**, *33*, 1775–1778. (d) Hammarström, L.; Barigelletti, F.; Flamigni, L.; Armaroli, N.; Sour, A.; Collin, J.-P.; Sauvage, J.-P. *J. Am. Chem. Soc.* **1996**, *118*, 11972–11973. (e) Barigelletti, F.; Flamigni, L.; Calogero, G.; Hammarström, L.; Sauvage, J.-P.; Collin, J.-P. *J. Chem. Soc., Chem. Commun.* **1998**, 2333–2334.

(2) (a) Grosshenny, V.; Harriman, A.; Gisselbrecht, J.-P.; Ziessel, R. *J. Am. Chem. Soc.* **1996**, *118*, 10315–10316. (b) Benniston, A. C.; Grosshenny, V.; Harriman, A.; Ziessel, R. *Angew. Chem., Int. Ed. Engl.* **1994**, *33*, 1884–1885. (c) Grosshenny, V.; Harriman, A.; Ziessel, R. *Angew. Chem., Int. Ed. Engl.* **1995**, *34*, 2705–2078. (d) Grosshenny, V.; Harriman, A.; Ziessel, R. *Angew. Chem., Int. Ed. Engl.* **1995**, *34*, 1100–1102. (e) El-ghayoury, A.; Harriman, A.; Khatyr, A.; Ziessel, R. *Angew. Chem., Int. Ed.* **2000**, *39*, 185–189. (f) Harriman, A.; Mayeux, A.; De Nicola, A.; Ziesel, R. *Phys. Chem. Chem. Phys.* **2002**, *4*, 2229–2235. (g) Hissler, M.; El-ghayoury, A.; Harriman, A.; Ziessel, R. *Angew. Chem., Int. Ed.* **1998**, *37*, 1717–1720. (h) Harriman, A.; Khatyr, A.; Ziessel, R.; Benniston, A. C. *Angew. Chem., Int. Ed.* **2000**, *39*, 4287–4290.

(3) (a) Schütte, M.; Kurth, D. G.; Linford, M. R.; Cölfen, H.; Möhwald, H. *Angew. Chem., Int. Ed.* **1998**, *37*, 2891–2893. (b) Barbieri, A.; Ventura, B.; Barigletti, F.; De Nicola, A.; Quesada, M.; Ziessel, R. *Inorg. Chem.* **2004**, *43*, 7359–7368. (c) Hjelm, J.; Handel, R. W.; Hagfeldt, A.; Constable, E. C.; Housecroft, C. E.; Forster, R. J. *Inorg. Chem.* **2005**, *44*, 1073–1081. (d) Flores-Torres, S.; Hutchison, G. R.; Soltzberg, L. J.; Abruna, H. D. *J. Am. Chem. Soc.* **2006**, *128*, 1513–1522.

(4) Balzani, V.; Scandola, F. *Supramolecular Photochemistry*; Ellis Horwood: Chichester, U.K., 1991.

(5) (a) Sauvage, J.-P.; Collin, J.-P.; Chambron, J.-C.; Guillerez, S.; Coudret, C.; Balzani, V.; Barigolletti, F.; De Cloa, L.; Flamigni, L. *Chem. Rev.* **1994**, *94*, 993–1019. (b) Harriman, A.; Ziessel, R. *Coord. Chem. Rev.* **1998**, *171*, 331–339. (c) Barigelletti, F.; Flamigni, L. *Chem. Soc. Rev.* **2000**, *29*, 1–12.

(6) Collin, J.-P.; Gaviña, P.; Heitz, V.; Sauvage, J.-P. *Eur. J. Inorg. Chem.* **1998**, *1*, 1–14.

(7) (a) Hagfeldt, A.; Grätzel, M. *Acc. Chem. Res.* **2000**, *33*, 269–277. (b) Bignozzi, R.; Argazzi, C. A.; Kleverlaan, C. J *Chem. Soc. Rev.* **2000**, *29*, 87–96. (c) Wang, P.; Zakeeruddin, S. M.; Moser, J. E.; Nazeeruddin, M. K.; Sekiguchi, T.; Grätzel, M. *Nat. Mater.* **2003**, *2*, 402–407. (d) Islam, A.; Sugihara, H.; Arakawa, H. *J. Photochem. Photobiol., A* **2003**, *158*, 131–138.

(8) (a) Slinker, J.; Bernards, D.; Houston, P. L.; Abruna, H. D.; Bernhard, S.; Malliaras, G. G. *Chem. Commun.* **2003**, 2392–2399. (b) Kalyuzhny, G.; Buda, M.; Mcneill, J.; Barbara, P.; Bard, A. J. *J. Am. Chem. Soc.* **2003**, *125*, 6272–6283. (c) Welter, S.; Brunner, K.; Hofstraat, J. W.; De Cola, L. *Nature* **2003**, *421*, 54–57.

10.1021/om700568h CCC: $40.75
Publication on Web 02/01/2008

Scheme 1. Structures of the Discussed Ferrocenyl-Bridged Ru^{2+} Complexes[a]

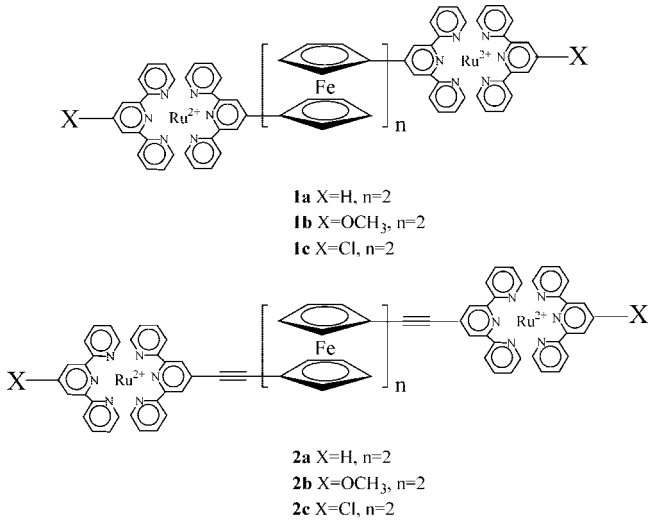

1a X=H, n=2
1b X=OCH_3, n=2
1c X=Cl, n=2

2a X=H, n=2
2b X=OCH_3, n=2
2c X=Cl, n=2

[a] In all cases, the counterion is PF_6^-.

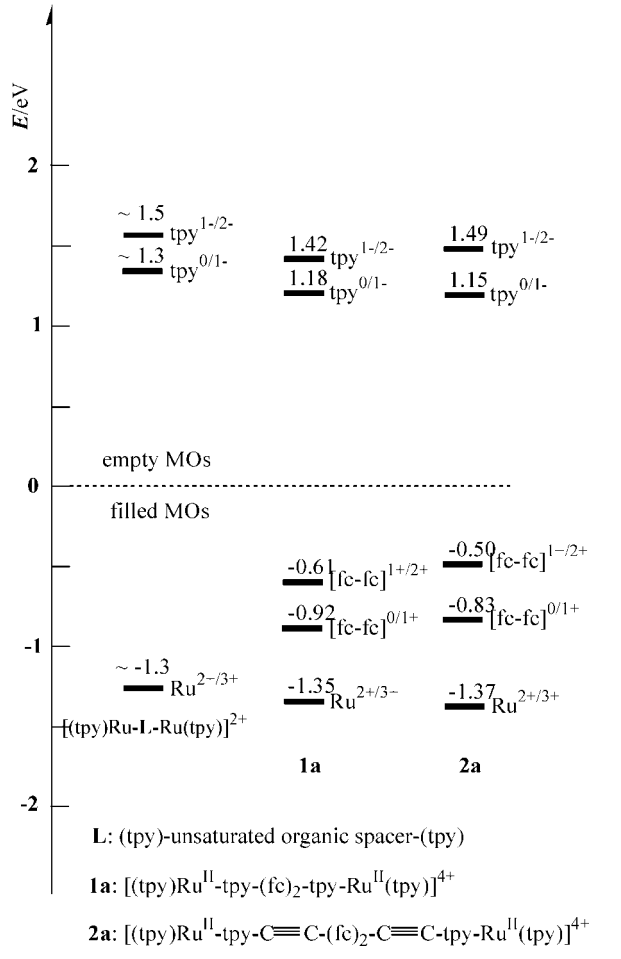

Figure 1. Electronic states probed by electrochemical measurements vs Ag/AgCl in CH_2Cl_2/CH_3CN (19:1) for $[Ru(tpy)_2]^{2+}$, **1a**, and **2a**.

$[Ru(tpy)_2]^{2+}$ was estimated previously from electrochemical measurements.[13] This means that the electrons cannot be easily phototransferred to the empty tpy molecular orbitals. From our previous electrochemical measurements, the filled ferrocenyl molecular orbitals lie close in energy to the empty tpy orbitals and electrons can be easily excited into ferrocenyl molecular orbitals.[9–12] Furthermore, the ferrocenyl spacer can be selectively oxidized to form a ferrocenium spacer. As shown in Scheme 2, rapid intramolecular photoelectron transfer between the two ruthenium centers in a mixed-valence diruthenium complex could occur through the oxidized ferrocenium spacer. Thus, an oxidized ferrocenium spacer, which possibly gives an effective π-delocalization along the main chain, can serve as a model system for a molecular wire.

Scheme 2. Intramolecular Photoelectron Transfer between the Two Ruthenium Centers in a Mixed-Valence Diruthenium Complex through an Oxidized Ferrocenium Spacer or through an Unsaturated Organic Spacer

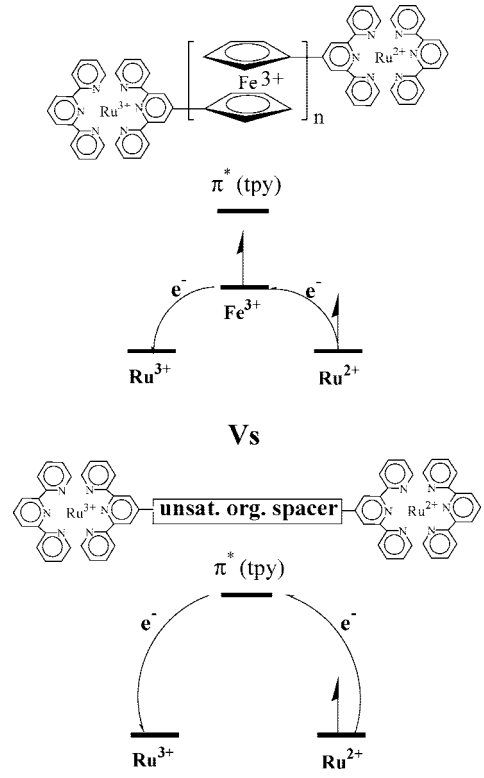

In our previous paper, the redox behavior of **1a** and **2a** (n = 2; Scheme 1) was dominated by the Ru^{2+}/Ru^{3+} redox couple ($E_{1/2}$ from 1.35 to 1.38 V), Fe^{2+}/Fe^{3+} redox couples ($E_{1/2}$ from 0.4 to 1.0 V) and $tpy/tpy^-/tpy^{2-}$ redox couples ($E_{1/2}$ from −1.3 to −1.5 V).[12] It is worth noting that a single irreversible wave was found for the Ru^{2+}/Ru^{3+} redox couple. This indicates that the electronic coupling between the two Ru^{2+} centers is relatively weak. In attempting to micromodulate the electronic communication between the terminal Ru^{2+} centers by manipulation of the energetics of the end-capping metal centers and the connecting spacer, we now describe the electrochemical and photophysical properties of **1b**,**c** and **2b**,**c** (Scheme 1).

(9) Dong, T.-Y.; Lin, M. C.; Chiang, Y. N. M.; Wu, J. Y. *Organometallics* **2004**, *23*, 3921–3930.

(10) Dong, T.-Y.; Chen, K.; Lin, M. C.; Lee, L. *Organometallics* **2005**, *24*, 4198–4206.

(11) Dong, T.-Y.; Chang, S. W.; Lin, S. F.; Lin, M. C.; Wen, Y. S.; Lee, L. *Organometallics* **2006**, *25*, 2018–2024.

(12) Dong, T.-Y.; Lin, M. C.; Chang, S. W.; Ho, C. C.; Lin, S. F.; Lee, L. *J. Organomet. Chem.* **2007**, *692*, 2324–2333.

(13) Hutchison, K.; Morris, J. C.; Nile, T. A.; Walsh, J. L.; Thompson, D. W.; Petersen, J. D.; Schoonover, J. R. *Inorg. Chem.* **1999**, *38*, 2516–2523.

Scheme 3. Synthesis of the Discussed 1,1′-Bis(ethynyl)-ferrocenyl-Bridged Ru^{2+}−tpy Complexes

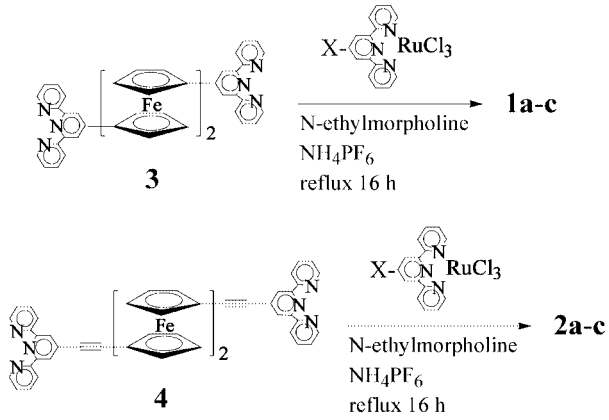

a: X=H; **b**: X=OCH_3; **c**: X=Cl

Experimental Section

General Information. All manipulations involving air-sensitive materials were carried out by using standard Schlenk techniques under an atmosphere of N_2. Solvents were dried as follows: THF and ether were distilled from Na/benzophenone; CH_2Cl_2 was distilled from CaH_2; diisopropylamine and TMEDA were distilled from KOH. Samples of 4′-chloro-2,2′:6′,2″-terpyridine and 4′-methoxyl-2,2′:6′,2″-terpyridine ligands were prepared according to the literature procedure.[14] Preparations of the biferrocenyl spacers (tpy-(fc)$_2$-tpy (**3**) and tpy-C≡C-(fc)$_2$-C≡C-tpy (**4**); fc = ferrocene) were described in previous papers.[9–12] As shown in Scheme 3, complexes **1a**−**c** and **2a**−**c** could be prepared.

Preparation of Compounds 1b,c and 2b,c. A stoichiometric amount of $RuLCl_3$ (0.10 mmol, L = 4′-chloro-2,2′:6′,2″-terpyridine or 4′-methoxyl-2,2′:6′,2″-terpyridine) in 30 mL of ethanol was added by means of a dropping funnel to an ethanol (30 mL) solution of corresponding **3** (0.05 mmol) or **4** (0.05 mmol) and 1 mL of *N*-ethylmorpholine. The mixture was then heated to reflux for 16 h. After the reaction mixture was cooled, the volume of ethanol solvent was reduced by half. A 10 mL aqueous solution of NH_4PF_6 (0.15 mmol) was added to give a violet-blue precipitate, which was collected by filtration.

In the case of **1b**, the crude product was chromatographed on activity V Al_2O_3, with acetone/CH_2Cl_2 (1:9) as eluent. The first band was starting material and undesired compounds. Continued elution with acetone/CH_2Cl_2 (2:8) afforded compound **1b**, which was recrystallized from acetone/ether (1:1). The yield of **1b** was 65%. ^{1}H NMR (d_3-acetonitrile) of **1b**: δ 8.50 (d, 8 Hz, 4H, OMe-tpy-$H_{3,3''}$); 8.46 (d, 8 Hz, 4H, Fc-tpy-$H_{3,3''}$); 8.35 (s, 4H, OMe-tpy-$H_{3',5'}$); 8.31 (s, 4H, Fc-tpy-$H_{3',5'}$); 7.91 (t, 7.5 Hz, 7.5 Hz, 8H, tpy-$H_{4,4''}$); 7.38 (d, 5.5 Hz, 4H, Fc-tpy-$H_{6,6''}$); 7.35 (d, 5.5 Hz, 4H, OMe-tpy-$H_{6,6''}$); 7.17 (dd, 5.8 Hz, 10 Hz, 8H, Fc-tpy-H and OMe-tpy-$H_{5,5''}$); 5.11 (s, 4H, Cp); 4.55 (s, 8H, Cp); 4.32 (s, 6H, OCH_3); 3.91 (s, 4H, Cp). ^{13}C NMR of **1b**: δ 167.76 (OMe-tpy-$C_{4'}$); 159.30 (Fc-tpy-$C_{2,2''}$); 159.16 (OMe-tpy-$C_{2,2''}$); 156.99 (OMe-tpy-$C_{2',6'}$); 155.72 (Fc-tpy-$C_{2',6'}$); 153.18 and 153.20 (Fc-tpy-C and OMe-tpy-$C_{6,6''}$); 149.03 (Fc-tpy-$C_{4'}$); 138.83 (OMe-tpy-$C_{4,4''}$); 138.48 (Fc-tpy-$C_{4,4''}$); 128.21 (OMe-tpy-$C_{5,5''}$); 128.10 (Fc-tpy-$C_{5,5''}$); 125.36 (OMe-tpy-$C_{3,3''}$); 125.24 (Fc-tpy-$C_{3,3''}$); 120.59 (Fc-tpy-$C_{3',5'}$); 111.60 (OMe-tpy-$C_{3',5'}$); 85.40 (s, Cp); 81.74 (s, Cp-C_1); 73.29 (s, Cp); 70.60 (s, Cp); 69.61 (s, Cp); 69.21 (s, Cp); 58.20 (s, OCH_3). Mass spectrum of **1b** (ESI): *m*/*z* 925.09 (calcd 925.57 for $[M - 2PF_6]^{2+}$); 569.06 (calcd 569.73 for $[M - 3PF_6]^{3+}$); 390.30 (calcd 391.31 for $[M - 4PF_6]^{4+}$). Anal. Calcd for **1b** ($C_{82}H_{62}F_{24}O_2Fe_2N_{12}P_4Ru_2$; M_w 2141.1616): C, 45.99; H, 2.92; N, 7.85. Found: C, 46.095; H, 3.065; N, 7.35.

In the case of **1c**, the crude product was chromatographed on activity V Al_2O_3, with acetone/CH_2Cl_2 (4:6) as eluent. The first band was starting material and undesired compounds. Continued elution with acetone/CH_2Cl_2 (6:4) afforded compound **1c**, which was recrystallized from acetone/ether (1:1). The yield of **1c** was 40%. ^{1}H NMR (d_3-acetonitrile) of **1c**: δ 8.86 (s, 2H, Cl-tpy-$H_{3',5'}$); 8.51 (d, 8.5 Hz, 2H, Cl-tpy-$H_{3,3''}$); 8.46 (d, 8 Hz, 2H, Fc-tpy-$H_{3,3''}$); 8.32 (s, 2H, Fc-tpy-$H_{3',5'}$); 7.96 (dd, 8.5 Hz, 8.5 Hz, 2H, Cl-tpy-$H_{4,4''}$); 7.92 (dd, 8 Hz, 7.5 Hz, 2H, Fc-tpy-$H_{4,4''}$); 7.42 (d, 5 Hz, 2H, Cl-tpy-$H_{6,6''}$); 7.34 (d, 5.5 Hz, 2H, Fc-tpy-$H_{6,6''}$); 7.25 (dd, 6.5 Hz, 6.5 Hz, 2H, Cl-tpy-$H_{5,5''}$); 7.15 (dd, 6.5 Hz, 6.5 Hz, 2H, Fc-tpy-$H_{5,5''}$); 5.12 (s, 4H, Cp); 4.57 (s, 8H, Cp); 3.92 (s, 4H, Cp). ^{13}C NMR of **1c**: δ 159.18 (Fc-tpy-C_2); 158.38 (Cl-tpy-C_2); 157.51 (Cl-tpy-$C_{2',6'}$); 155.32 (Fc-tpy-$C_{2',6'}$); 153.64 (Fc-tpy-$C_{6,6''}$); 153.31 (Cl-tpy-$C_{6,6''}$); 150.25 (Fc-tpy-$C_{4'}$); 143.51 (Cl-tpy-$C_{4'}$); 139.24 (Cl-tpy-$C_{4,4''}$); 138.99 (Fc-tpy-$C_{4,4''}$); 128.90 (Cl-tpy-$C_{5,5''}$); 128.27 (Fc-tpy-$C_{5,5''}$); 125.97 (Cl-tpy-$C_{3,3''}$); 125.58 (Fc-tpy-$C_{3,3''}$); 125.08 (Cl-tpy-$C_{3',5'}$); 120.88 (Fc-tpy-$C_{3',5'}$); 85.60 (s, Cp); 81.72 (s, Cp-C_1); 73.61 (s, Cp); 70.81 (s, Cp); 69.88 (s, Cp); 69.40 (s, Cp). Mass spectrum of **1c** (ESI): *m*/*z* 930.0 (calcd 930.52 for $[M - 2PF_6]^{2+}$); 571.70 (calcd 572.36 for $[M - 3PF_6]^{3+}$); 393.03 (calcd 393.28 for $[M - 4PF_6]^{4+}$). Anal. Calcd for **1c** ($C_{80}H_{56}F_{24}Cl_2Fe_2N_{12}P_4Ru_2$, M_w 2150.0182): C, 44.69; H, 2.63; N, 7.87. Found: C, 8.04; H, 44.715; N, 2.68.

In the case of **2b**, the crude product was purified directly by recrystallization from acetone/ether (1:1). The yield of **2b** was 86%. ^{1}H NMR (d_3-acetonitrile) of **2b**: δ 8.59 (s, 4H, ethynylene-tpy-$H_{3',5'}$); 8.49 (t, 7.5 Hz, 8H, ethynylene-tpy and tpy-$H_{3,3''}$); 8.35 (s, 4H, tpy-$H_{3',5'}$); 7.94 (ddd, 7.9 Hz, 7.9 Hz, 1.0 Hz, 4H, ethynylene-tpy-$H_{4,4''}$); 7.90 (ddd, 8.5 Hz, 8.5 Hz, 1.3 Hz, 4H, tpy-$H_{4,\ 4''}$); 7.44 (dd, 5 Hz, 0.5 Hz, 4H, ethynylene-tpy-$H_{6,6''}$); 7.33 (dd, 4.8 Hz, 0.5 Hz, 4H, tpy-$H_{6,6''}$); 7.21 (td, 6.6 Hz, 1.3 Hz, 4H, ethynylene-tpy-$H_{5,5''}$); 7.13 (td, 6.5 Hz, 1.2 Hz, 4H, tpy-$H_{5,5''}$); 4.78 (t, 4H, Cp); 4.55 (t, 4H, Cp); 4.39 (t, 4H, Cp); 4.35 (t, 4H, Cp); 4.32 (s, 6H, −OCH_3). ^{13}C NMR of **2b**: δ 58.40 (s, −OCH_3); 65.13 (s, Cp-C_1); 69.47 (s, Cp); 70.90 (s, Cp-C); 72.31 (s, Cp); 74.08 (s, Cp); 84.86 (s, tpy-C′); 86.00 (s, Cp-$C_{1'}$); 98,79 (s, ≡C-Cp); 111.83 (s, tpy-$C_{3',5'}$); 125.41 (s, ethynylene-tpy-$C_{3',5'}$); 125.56 (s, tpy-$C_{3,3''}$); 125.65 (s, ethynylene-tpy-$C_{3,3''}$); 128.49 (s, tpy-$C_{5,5''}$); 128.69 (s, ethynylene-tpy-$C_{5,5''}$); 131.54 (s, ethynylene-tpy-$C_{4'}$); 139.00 (s, tpy-$C_{4,4''}$); 139.12 (s, ethynylene-tpy-$C_{4,4''}$); 153.40 (s, tpy-$C_{6,6''}$); 153.71 (s, ethynylene-tpy-$C_{6,6''}$); 156.70 (s, tpy-$C_{2',6'}$); 156.91 (s, ethynylene-tpy-$C_{2',6'}$); 158.94 (s, tpy-$C_{2,2''}$); 159.11 (s, ethynylene-tpy-$C_{2,2''}$); 168.27 (s, tpy-$C_{4'}$). Mass spectrum of **2b** (ESI): *m*/*z* 950.09 (calcd 950.57 for $[M - 2PF_6]^{2+}$); 585.06 (calcd 585.73 for $[M - 3PF_6]^{3+}$); 402.52 (calcd 403.31 for $[M - 4PF_6]^{4+}$). Anal. Calcd for **2b** ($C_{86}H_{62}N_{12}O_2Fe_2Ru_2P_4F_{24}$; M_w 2189.1789): C, 47.18; H, 2.85; N, 7.67. Found: C, 47.35; H, 3.13; N, 7.17.

For **2c**, the crude product was chromatographed on activity V Al_2O_3, with CH_2Cl_2 as eluent. The first band was starting material and undesired compounds. Continued elution with acetone afforded compound **2c**, which was recrystallized from acetone/ether (1:1). The yield of **2c** was 50%. ^{1}H NMR (d_3-acetonitrile) of **2c**: δ 8.87 (s, 4H, tpy-$H_{3',5'}$); 8.63 (s, 4H, ethynylene-tpy-$H_{3',5'}$); 8.51 (d, 8.5 Hz, 8H, ethynylene-tpy and tpy-$H_{3,3''}$); 7.94 (t, 7.5 Hz, 8H, ethynylene-tpy and tpy-$H_{4,4''}$); 7.39 (t, 6 Hz, 5.5 Hz, 8H, ethynylene-tpy and tpy-$H_{6,6''}$); 7.21 (d, AB, 8 Hz, 4H, ethynylene-tpy or tpy-$H_{5,5''}$); 7.18 (d, AB, 7.5 Hz, 4H, ethynylene-tpy or tpy-$H_{5,5''}$); 4.79 (t, 1.5 Hz, 4H, Cp); 4.55 (t, 1.5 Hz, 4H, Cp); 4.39 (t, 1.5 Hz, 4H, Cp); 4.35 (t, 1.5 Hz, 4H, Cp). ^{13}C NMR (d_3-acetonitrile): δ 65.02 (s, Cp-C_1); 69.50 (s, Cp); 70.93 (s, Cp); 72.37 (s, Cp); 74.14 (s, Cp); 84.78 (s, tpy-C≡); 86.03 (s, Cp-$C_{1'}$); 99.34 (s, ≡C-Cp); 125.18 (s, tpy-$C_{3',5'}$); 125.63 (s, tpy-$C_{3,3''}$ or ethynylene-tpy-$C_{3,3''}$); 125.84 (s, ethynylene-tpy-$C_{3',5'}$); 126.03 (s, tpy-$C_{3,3''}$ or ethynylene-tpy-

(14) Constable, E. C.; Cargill Thompson, A. M. W. *New J. Chem.* **1992**, *16*, 855–867.

$C_{3,3''}$); 128.68 (s, tpy-$C_{5,5''}$ or ethynylene-tpy-$C_{5,5''}$); 129.01 (s, tpy-$C_{5,5''}$ or ethynylene-tpy-$C_{5,5''}$); 132.57 (s, ethynylene-tpy-$C_{4'}$); 139.33 (s, tpy-$C_{4,4''}$ and ethynylene-tpy-$C_{4,4''}$); 144.07 (s, tpy-$C_{4'}$); 153.68, 153.71 (s, tpy-$C_{6,6''}$ and ethynylene-tpy-$C_{6,6''}$); 156.14 (s, ethynylene-tpy-$C_{2',6'}$); 157.24 (s, tpy-$C_{2',6'}$ or tpy-$C_{2,2''}$); 158.16 (s, tpy-$C_{2',6'}$ or tpy-$C_{2,2''}$); 158.69 (s, ethynylene-tpy-$C_{2,2''}$). Mass spectrum of **2c** (ESI): *m*/*z* 587.73 (calcd 588.36 $[M - 3PF_6]^{3+}$); 404.53 (calcd 405.28 $[M - 4PF_6]^{4+}$). Anal. Calcd for **2c** ($C_{84}H_{56}N_{12}Fe_2Ru_2Cl_2P_4F_{24}$; M_w 2198.0164); C, 45.90; H, 2.57; N, 7.65. Found: C, 45.06; H, 2.71; N, 7.73.

Physical Measurements. ^{1}H NMR spectra were run on a Varian INOVA 500 MHz spectrometer. Mass spectra were obtained with a VG-BLOTECH-QUATTRO 5022 system, and ESI-LCQ mass spectra were obtained with a Thermo Finnigan spectrometer. Electrochemical measurements were carried out with a CHI 660B system. Voltammetry measurements were performed with a stationary glassy-carbon working electrode. These experiments were carried out with a 1×10^{-3} M solution of dried CH_2Cl_2 containing 0.1 M of $(n\text{-}C_4H_9)_4NPF_6$ as supporting electrolyte. The potentials quoted in this work are relative to an Ag/AgCl electrode or to an Ag-wire electrode at 25 °C. Under these conditions, ferrocene showed a reversible one-electron redox wave ($E_{1/2} = 0.50$ V). Emission spectra were measured with a Hitachi F4500 photon-counting spectrofluorometer equipped with a red-sensitive R928F photomultiplier tube. Wavelengths were corrected using $[Ru(bpy)_3]^{2+}$ as the reference standard ($\lambda_{max}^{em} = 607$ nm). Quantum yields (Φ) were measured ($\lambda_{exc} = 490$ nm) in optically dilute H_2O/CH_3CN (4/1) solution (5×10^{-6} M) at room temperature relative to $[Ru(bpy)_3]^{2+}$, for which $\Phi = 0.059$. Luminescence lifetimes were measured by OB920 time-resolved fluorescence spectroscopy with an nF 900 ns Flashlamp (Edinburgh Instruments Ltd.) with a time-correlated, single-photon counting methodology following excitation at 340 nm. UV spectra were recorded from 250 to 800 nm in CH_3CN by using 1.0 cm quartz cells with a Hitachi U-4001 spectrophotometer.

Structure Determination of 4. A red crystal ($0.10 \times 0.08 \times 0.06$ mm) was grown when a layer of hexane was allowed to slowly diffuse into a CH_2Cl_2 solution of **4**. The single-crystal X-ray determination of compound **4** with Mo Kα radiation was carried out at 100.0(1) K by using an Enraf-Nonius CAD4 diffractometer. Data were collected to a maximum 2θ value of 50.06°. Of the 15 712 reflections collected, there were 3533 independent reflections ($R_{int} = 0.0877$) with $F_o^2 > 2.0\sigma(F_o^2)$. A semiempirical absorption correction based on azimuthal scans of several reflections was applied. The structures were solved by an expanded Fourier technique. All non-hydrogen atoms were refined anisotropically. Hydrogen atoms were included at an ideal distance. Complete tables of the X-ray crystal data, the final positional parameters for all atoms, the bond distances and angles, and thermal parameters of compound **4** are given in the Supporting Information.

Results and Discussion

Synthesis and Characterization. Binuclear Ru(II) complexes of **1a**−**c** and **2a**−**c** were prepared by reacting biferrocenylalkynyl spacers (**3** or **4**) with 1–1.1 equiv of $Ru(tpy)Cl_3$ (Scheme 3). The higher yields obtained in the synthesis of **1a**−**c** and **2a**−**c** prompted us to use *N*-ethylmorpholine as the reducing agent instead of triethylamine, the compound generally used to prepare $[Ru(tpy)_2]^{4+}$ derivatives.[15] Complexes were isolated as the PF_6^- salts and purified by column chromatography. All complexes were characterized by 1D and 2D NMR techniques, elemental analysis, and ESI-MS given as Supporting Information. In this study, NMR characterization of **1b**,**c** and **2b**,**c** in

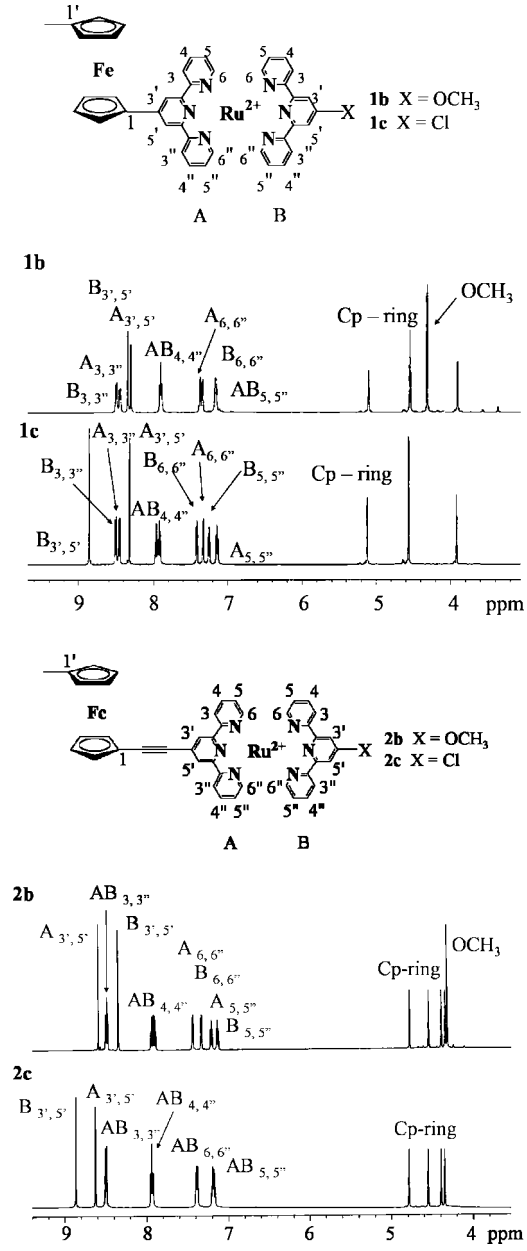

Figure 2. ^{1}H NMR spectra of **1b**,**c** (top) and **2b**,**c** (bottom).

CD_3CN was achieved by utilization of $^1H-^1H$ and $^1H-^{13}C$ COSY and HMBC 2D NMR techniques. As shown in Figure 2, the ^{1}H NMR spectra of **1b**,**c** and **2b**,**c** exhibit several signals at low field corresponding to the tpy ligands. The spectra of **1b**,**c** were characterized by a singlet corresponding to the 4′-X-tpy-$H_{3',5'}$ (X = OCH_3, Cl) protons and a singlet corresponding to the cp-tpy-$H_{3',5'}$ protons, which have long-range interactions with the cyclopentadienyl carbon. In the case of **2b**,**c**, the spectra were characterized by a singlet corresponding to the 4′-X-tpy-$H_{3',5'}$ protons and a singlet corresponding to the ethynyl-tpy-$H_{3',5'}$ protons, which have long-range interactions with the ethynyl carbon.

Molecular Structure of 4. The X-ray structure of **4** showed that it is in the space group $P2_1/c$ at 100 K. Complete tables of positional parameters, bond distances, and bond angles are given as Supporting Information. As shown in Figure 3, the ORTEP view confirms the molecular structure, with the ferrocenyl group directly linked to the acetylene linkage which is linked to the 4′-position of the 2,2′:6′,2″-terpyridine. The biferrocenyl moiety exists in a trans conformation,with the two iron ions on opposite

(15) Sullivan, B. P.; Calvert, J. M.; Meyer, T. *Inorg. Chem.* **1980**, *19*, 1404–1407.

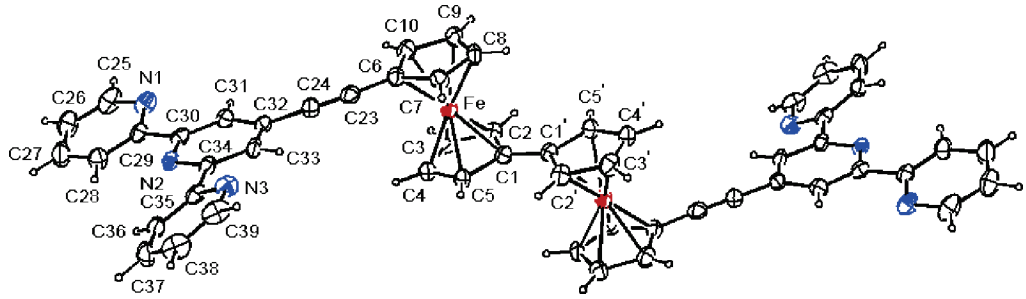

Figure 3. ORTEP drawing of **4** with the atom-numbering scheme. Selected bond distances (Å) and angles (deg): Fe−C1, 2.051(3); Fe−C2, 2.038(3); Fe−C3, 2.028(3); Fe−C4, 2.037(3); Fe−C5, 2.025(3); Fe−C6, 2.047(3); Fe−C7, 2.019(3); Fe−C8, 2.024(3); Fe−C9, 2.036(3); Fe−C10, 2.043(3); C6−C23, 1.427(4); C23−C24, 1.193(4); C6−C23−C24, 176.4(3); C23−C24−C32, 178.8(4).

Table 1. Comparison of Selected Atomic Distances (Å) and Angles (deg)

	3 (*Pbca* phase)[f]	**3** (*C*2/*c* phase)[f]	**4**
Fe−C[a]	2.043	2.04	2.035(3)
Fe−Cp[b]	1.65	1.64	1.64
Cp−Cp[c]	2.5	1.33	2.7(1)
Cp−tpy[d]	11.87	19.19	6.00
tpy−tpy[e]	14.52; 9.18	5.96; 6.75	12.54; 22.85

[a] Average Fe−C distance for each ferrocenyl moiety. [b] Distance from the Fe atom to the center of mass of the Cp ring in each ferrocenyl moiety. [c] Dihedral angle between the two least-squares-fitted Cp rings in each ferrocenyl moiety. [d] Dihedral angle between the Cp ring and the central ring of the terpyridine moiety. [e] Dihedral angle between the central ring and the terminal ring for each terpyridine moiety. [f] From ref 9.

sides of the fulvalenide ligand. The two least-squares-fitting Cp planes in a given ferrocenyl moiety are nearly parallel, and the dihedral angle is 2.7(1)°. Inspection of the average distances of Fe−C (2.035(3) Å) and Fe−Cp (1.64 Å) indicates that the metallocenes are in the Fe^{2+} oxidation state. The bonds and angles about the Cp rings vary little, and they are close to those reported for analogous ferrocenes.[16] Furthermore, the two Cp rings associated with the Fe center are nearly eclipsed, with average staggering angles of 12.62°. Attachment of a terpyridylethynyl moiety to the 1′-position of biferrocene has minimal influence on the molecular structure, in comparison with the case for the analogous biferrocene.[17] The average C−C triple-bond distance (1.194(9) Å) in the ethynyl moiety is in agreement with that (1.198 Å) reported for an analogous C−C triple bond.[18]

The 2,2′:6′,2″-terpyridine group adopts the expected trans−trans conformation about the interannular C29−C30 and C34−C35 bonds. The pyridyl units in each terpyridine group are not completely coplanar, and the dihedral angles range from 12.54 to 22.85° with an average value of 18.08°. The Cp ring of the ethynyl−Cp group is nearly coplanar with the central pyridyl ring of terpyridine, and the dihedral angle is 6.00°.

A direct comparison was made between **3** and **4** (Table 1). In a previous paper,[9] we found that compound **3** exhibited two crystalline morphologies at room temperature. Red crystals in the *Pbca* phase were grown when a layer of hexane was allowed to slowly diffuse into a CH_2Cl_2 solution of **3**. Orange-red crystals in the *C*2/*c* phase were obtained when a layer of cyclohexane was allowed to slowly diffuse into a CH_2Cl_2 solution of **3**. A comparison of structural features between the two different crystallographic phases of **3** is interesting. The tpy substituent on the Cp ring is situated differently. The two tpy substituents in the *Pbca* phase show a cisoid conformation relative to the fulvalenide ligand. However, in the case of the *C*2/*c* phase, the two tpy substituents show a transoid conformation relative to the fulvalenide ligand. In the case of **4**, only one crystalline morphology in the $P2_1/c$ phase has been found and the two terpyridylethynyl substituents show a transoid conformation relative to the fulvalenide ligand. The acetylene linkage in **4** would allow the tpy moiety to have more conformational freedom than that in **3**, resulting in a larger dihedral angle between the central ring and the terminal ring for each terpyridine moiety (tpy−tpy values given in Table 1).

Electrochemical Measurements for 1b,c and 2b,c. When the CV measurements were recorded at potentials from 0.0 to 1.6 V with Ag/AgCl as a reference electrode, they underwent two quasi-reversible ferrocene-based one-electron oxidations and an irreversible Ru^{2+}-based redox wave. The cathodic wave was small or vanishing when the scanning turned back. Extracted electrochemical data and cyclic voltammograms with Ag/AgCl as a reference electrode for these complexes are given as Supporting Information. Therefore, Ag wire as a pseudo-reference electrode was employed to obtained better-resolved potential information for the Ru^{2+}/Ru^{3+} redox couple in this study. The electrochemical results for **1b**,**c**, **2b**,**c**, and related compounds are given in Table 2. As expected, the room-temperature cyclic voltammograms (CV) of **1b**,**c** and **2b**,**c** are respectively similar to those for **1a** and **2a** reported previously.[12] The redox behavior is dominated by the irreversible Ru^{2+}/Ru^{3+} redox couple ($E_{1/2}$ at ∼1.35 V), Fe^{2+}/Fe^{3+} redox couples ($E_{1/2}$ from 0.33 to 0.98 V), and tpy/tpy^{-}/tpy^{2-} redox couples ($E_{1/2}$ from −1.14 to −1.49 V). When the CV measurements were recorded at potentials from 0.0 to 1.2 V, they underwent two ferrocene-based one-electron oxidations. At room temperature, when the scanning potential was increased to 1.6 V, an irreversible Ru^{2+}-based oxidation developed. Figure 4 shows typical cyclic voltammograms of **2b**, from which it is clear that there are two main Fe^{2+}/Fe^{3+} redox couples at half-potentials of 0.60 and 0.96 V vs Ag wire with the separation $\Delta E = 0.36$ V and two tpy/tpy^{-}/tpy^{2-} redox couples at $E_{1/2} = -1.08$ and −1.39 V. Under the CV conditions, the $Ru^{2+/3+}$ $E_{1/2}$ potential cannot be easily or accurately extracted. Voltammograms of **1a**,**c** and **2a**,**c** are also given as Supporting Information.

During electrolysis of **1a**,**c** and **2a**,**c** at room temperature in anhydrous CH_2Cl_2 under the CV conditions, the electrode surface was coated with a dark red, strongly adherent polymeric film. Polymerization was obvious if the binuclear Ru^{2+} complexes contained a chloride substituent or ethynyl group. Therefore, differential pulse voltammetry (DPV) was also employed to obtain better-resolved potential information in this

(16) Seiler, P.; Dunitz, J. D. *Acta Crystallogr., Sect. B* **1979**, *35*, 1068–1074.

(17) Dong, T.-Y.; Huang, C. H.; Chang, C. K.; Wen, Y. S.; Lee, S. L.; Chen, J. A.; Yeh, W. Y.; Yeh, A. *J. Am. Chem. Soc.* **1993**, *115*, 6357–6368.

(18) Siemeling, U.; der Brüggen, J. V.; Vorfeld, U.; Neumann, B.; Stammler, A.; Stammler, H.-G.; Brockhinke, A.; Plessow, R.; Zanello, P.; Laschi, F.; de Biani, F. F.; Fontani, M.; Steenken, S.; Stapper, M.; Gurzadyan, G. *Chem. Eur. J.* **2003**, *9*, 2819–2833.

Table 2. DPV Data of 1a−c, 2a−c, and Related Compounds at a Scan Rate of 100 mV s^{-1}

compd	$Ru^{2+/3+}$ $E_{1/2}$ (V)[a]	$Fe^{2+/3+}$ $E_{1/2}$ (V)[a]	$\Delta E_{1/2}$ (V)[b]	$tpy^{0/-/2-}$ $E_{1/2}$ (V)[a]	$\Delta E_{1/2}$ (V)[b]
ferrocene		0.50			
$[Ru(tpy)_2]^{2+}$ [c]	1.27			−1.27	0.24
				−1.51	
3		0.54	0.45		
		0.99			
4		0.79	0.40		
		1.19			
1a	1.30	0.48	0.32	−1.28	0.32
		0.80		−1.60	
1b	1.24	0.49	0.32	−1.32	0.27
		0.81		−1.59	
1c	1.32	0.46	0.34	−1.18	0.37
		0.80		−1.55	
2a	1.37[d]	0.49	0.37	−1.11	0.37
		0.86		−1.48	
2b	1.37	0.59	0.35	−1.06	0.34
		0.94		−1.40	
2c	1.58[d]	0.63	0.35	−0.95	0.29
		0.99		−1.24	

[a] All half-wave potentials are referenced to an Ag-wire electrode in anhydrous CH_2Cl_2 solution. [b] The difference of $E_{1/2}$ values between two redox waves of ferrocenyl moieties. [c] From ref 13. [d] Irreversible.

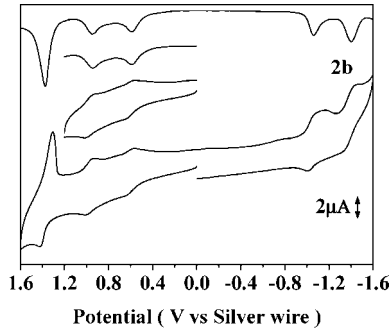

Figure 4. Electrochemical measurements of **2b** in CH_2Cl_2 at room temperature vs Ag wire.

study, because the $Ru^{2+/3+}$ redox process for the series of multinuclear complexes was poorly reversible in the CV experiment. In this study, DPV measurements of **1a**−**c** and **2a**−**c** were obtained in anhydrous CH_2Cl_2 solution. The redox potentials from DPV measurements are given in Table 2. As shown in Figure 4, the reversible peak at half-potential of 1.37 V from DPV is assigned to the $Ru^{2+/3+}$ redox couple in **2b**. Furthermore, two main Fe^{2+}/Fe^{3+} redox couples at half-potentials of 0.59 and 0.94 V vs Ag wire with the separation $\Delta E = 0.35$ V and two $tpy/tpy^{-}/tpy^{2-}$ redox couples at $E_{1/2} = -1.06$ and −1.40 V were found. The following discussion is based on the data extracted from the DPV measurements.

As shown in Table 2, attachment of a $-OCH_3$ or −Cl moiety to the 4′-position of tpy in the Ru^{2+} complexes **1b**,**c** and **2b**,**c** has an influence on the Ru^{2+}/Ru^{3+} redox potential. The effect of the substituent on the stability of the metal center is illustrated by the shift of the half-wave potential. In general, electron-donating groups stabilize the cation, lowering the half-wave potential, while electron-withdrawing groups have the opposite effect. The Ru^{2+}-centered oxidation processes in the Cl-substituted complexes **1c** and **2c** are shifted more positively compared to those of **1a** and **2a**, respectively. Comparing the Ru^{2+}/Ru^{3+} redox potential in **1b** with that in **1a**, we indeed observed that the Ru^{2+}/Ru^{3+} metal center in **1b** (1.24 V) was more easily oxidized than that in **1a** (1.30 V). Interestingly, the attachments of $-OCH_3$ and −Cl moieties to the tpy in the Ru^{2+} complexes **1b**,**c** had no influence on the Fe^{2+}/Fe^{3+} redox potentials, but more a positive shift was observed in comparing the Fe^{2+}/Fe^{3+} $E_{1/2}$ potentials of **2b** (0.59, 0.94 V) and **2c** (0.63, 0.99 V) with those of **2a** (0.49, 0.86 V). The positive potential shift observed for the insertion of an ethynylene group into the main chain, respectively giving **2b**,**c**, is attributed to the more pronounced electron delocalization in the extended π orbitals included in the ferrocenyl subunits. Furthermore, both $-OCH_3$ and −Cl substitutents show electron-withdrawing electronic effects. In fact, it is noted that the $-OCH_3$ substituent in **2b** does not have an electron-donating electronic effect on the Ru^{2+}/Ru^{3+} redox potential, om comparison of the Ru^{2+}/Ru^{3+} $E_{1/2}$ value of **2b** (1.37 V) with that of **2a** (1.37 V). The same electronic effects were also observed on the $tpy/tpy^{-}/tpy^{2-}$ redox potentials.

Although the Ru^{2+}/Ru^{3+}, Fe^{2+}/Fe^{3+}, and $tpy/tpy^{-}/tpy^{2-}$ redox potentials were micromodulated by the attachment of $-OCH_3$ and −Cl substitutents, a single wave was found for the Ru^{2+}/Ru^{3+} redox couple in the electrochemical measurements of **1b**,**c** and **2b**,**c**. A fact indicates that the electronic coupling between the Ru^{2+} centers is still relatively weak.

UV–Visible Spectroscopy. The visible spectra for Ru^{2+}−tpy complexes (**1b**,**c** and **2b**,**c**) are dominated by $^1[(d(\pi)_{Ru})^6] \rightarrow {}^1[d(\pi)^5(\pi^*_{tpy})^1]$ MLCT absorption bands from 482 to 494 nm, which were assigned by analogy to the well-documented MLCT transitions found for $[Ru(tpy)_2]^{2+}$ (472 nm), $[Ru(tpy)(fctpy)]^{2+}$ (478 nm), and $[Ru(fctpy)_2]^{2+}$ (482 nm).[13,18–21] This assignment was supported by the electrochemical measurements. The potential difference of $E_{1/2}$ between the Ru^{2+}/Ru^{3+} redox couple and the first tpy/tpy^{-} redox couple is in the region from 2.43 to 2.58 ± 0.01 V, which is in response from 511 to 481 ± 12 nm. Furthermore, the MLCT absorption bands are broad because they include a series of MLCT transitions. Well-defined shoulders on the $^1[(d(\pi)_{Ru})^6] \rightarrow {}^1[d(\pi)^5(\pi^*_{tpy})^1]$ MLCT band were observed for the monomeric $[Ru(tpy)_2]^{2+}$. These shoulders have been previously assigned to $^1[(d(\pi)_{Ru})^6] \rightarrow {}^3[d(\pi)^5(\pi^*_{tpy})^1]$ MLCT.[20,21] Computer deconvolution of this broad MLCT absorption band with four Gaussian lines was carried out.[12,13] The resulting fitting data for these absorptions are collected in Table 3. Figure 5 shows representative UV spectra of **2a**−**c**. UV spectra of **1a**−**c** are given as Supporting Information. From Table 3, the ^{1}MLCT bands of **1b**,**c** and **2b**,**c** are slightly red-shifted by the attachment of $-OCH_3$ and −Cl substituents, respectively, in comparison with those of **1a** and **2a**.

From computer deconvolution, absorption bands at 576 nm for **1b**, 572 nm for **1c**, 579 nm for **2b**, and 568 nm for **2c** are apparent in the visible region. In the case of Ru^{2+} transition-metal complexes containing ferrocenyl moieties, an intense broad structureless band in the ∼520 nm region has been observed.[5,13,22] For the $[Ru(fctpy)_2]^{2+}$ compound, a band at 526 nm is apparent.[13,18] This band has been assigned to the $^1[(d(\pi)_{Fe})^6] \rightarrow {}^1[(d(\pi)_{Fe})^5(\pi^*_{tpy}{}^{Ru})^1]$ transition.[13] In our studies, this band is not present in the parent neutral compounds but upon coordination with Ru^{2+} metal centers rises to a more intense transition in the visible region.

In electrochemical measurements, the potential difference of $E_{1/2}$ between the first Fe^{2+}/Fe^{3+} redox couple and the first tpy/tpy^{-} redox couple is in the region from 1.58 to 1.81 ± 0.01 V, which is in response from 786 to 686 ± 12 nm. We observed that the $^1[(d(\pi)_{Fe})^6] \rightarrow {}^1[(d(\pi)_{Fe})^5(\pi^*_{tpy}{}^{Ru})^1]$ transition occurred

(19) Braddock, J. N.; Meyer, T. J. *J. Am. Chem. Soc.* **1973**, *95*, 3158–3162.
(20) Kober, E. M.; Meyer, T. J. *Inorg. Chem.* **1982**, *21*, 3967–3977.
(21) Coe, B. J.; Thompson, D. W.; Culbertson, C. T.; Schoonover, J. R.; Meyer, T. J. *Inorg. Chem.* **1995**, *34*, 3385–3395.
(22) Benniston, A. C.; Goulle, V.; Harriman, A.; Lehn, J.-M.; Marczinke, B. *J. Phys. Chem.* **1994**, *98*, 7798–7804.

Table 3. UV–Visible Absorption Data

compd	abs (nm) (ϵ ($\times 10^{-3}$ M^{-1} cm^{-1}))[a]			
	tpy	Ru-based		Fe-based
	$\pi \rightarrow \pi^*$	^{1}MLCT	^{3}MLCT	^{1}MLCT
$[Ru(tpy)_2][PF_6]_2$[b]	270 (36), 308 (51)	472 (14)	435 (7.9), 472 (14)	
$[Ru(fctpy)_2][PF_6]_2$[b]	274 (49), 284 (44)	482 (15)		526 (15)
1a[c]	274 (117), 308 (117)	482 (53)	438 (30), 524 (17)	555 (13)
1b[d]	272 (125), 304 (149)	484 (50)	453 (38), 523 (38)	576 (26)
1c[d]	274 (115), 308 (122)	482 (33)	440 (19), 534 (21)	572 (26)
2a[c]	273 (129), 307 (123)	486 (37)	445 (21), 529 (23)	571 (13)
2b[d]	273 (97), 304 (111)	494 (42)	451 (26), 535 (25)	579 (12)
2c[d]	275 (120), 308 (140)	488 (50)	448 (27), 528 (31)	568 (17)

[a] In acetonitrile solution at room temperature. [b] From ref 13. [c] From ref 12. [d] This work.

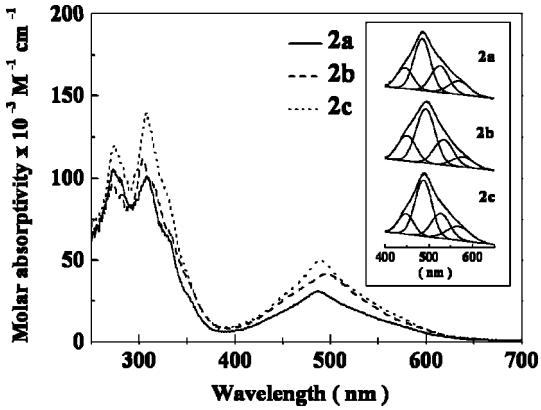

Figure 5. UV–visible absorption spectra of Ru^{2+} complexes **2a**−**c**. Inset: computer deconvolution for **2a**−**c**.

Table 4. Room-Temperature Luminescence Data

compd	emission (nm)[a]				
	λ_{max}	Φ ($\times 10^4$)	τ (ns)	k_r ($\times 10^{-3}$ s^{-1})[b]	k_{nr} ($\times 10^{-7}$ s^{-1})[b]
2a	690	1.48	67	2.2	4.2
2b	696	1.09	16	6.8	6.2
2c	648	0.45	18	2.4	5.3

[a] Conditions and definitions: in H_2O/CH_3CN (4:1) solution at room temperature; λ_{max}, emission maximum; Φ, emission quantum yield (measured at λ_{exc} = 490 nm); τ, triplet lifetime (measured at λ_{exc} = 340 nm)). [b] From $= k_{nr}/(k_{nr} + k_{nr})$, where k_r and k_{nr} represent the rate constants for radiative and nonradiative decay with $k_r = \Phi/\tau$ and $k_{nr} = 1/\tau - k_r$.

at a much higher energy region. This discrepancy may be a consequence of the fact that electrochemical measurements probe the ground state of the redox-active species involved, whereas UV/vis spectroscopy probes excited states. The time scale of electrochemical measurement, which is equal to the experimental time of measurement, is absolutely greater than that of the UV/vis technique ($\sim 10^{-16}$ s). In electrochemical measurements, a change in oxidation state for a transition-metal complex is generally accompanied by a coordination sphere reorganization. When the ferrocenyl moiety is oxidized, the two Cp rings bound to the Fe(II) ion (Fe^{II}−Cp = 1.65 Å)[16] move away from the metal to adjust their distance to the larger dimension appropriate for a $(Cp)_2Fe^{III}$ moiety (Fe^{III}−Cp = 1.70 Å).[23] During the reduction process, the dimension of the $(Cp)_2Fe^{III}$ moiety contracts to that of a $(Cp)_2Fe^{II}$ moiety. The electronic ground state of ferrocene is a singlet, $^1A_{1g}$ ($e_{2g}{}^4a_{1g}{}^2$), where the one-electron molecular orbitals are predominantly d orbital in character: the higher energy state of a_{1g} (d_{z^2}) and lower energy state of e_{2g} ($d_{x^2-y^2}$, d_{xy}).[24] However, the electronic ground state of ferrocenium is a doublet, $^2E_{2g}$ ($a_{1g}{}^2e_{2g}{}^3$), where the one-electron a_{1g} (d_{z^2}) molecular orbital is at a lower energy state and the one-electron e_{2g} ($d_{x^2-y^2}$, d_{xy}) molecular orbitals are at a higher energy state. In other words, electrochemical measurements probe the energetics of the electronic ground states of $^1A_{1g}$ and $^2E_{2g}$ involved. In UV/vis measurements, the electron transfer process is not accompanied by the coordination sphere reorganization on the basis of the Franck–Condon principle and these measurments probe the energetics of the electronic ground state of $^1A_{1g}$ (Fe center, $e_{2g}{}^4a_{1g}{}^2$; tpy center, $(\pi^*)^0$) and the excited state of $^1A_{1g}$ (Fe center, $e_{2g}{}^4a_{1g}{}^1$; tpy center, $(\pi^*)^1$).

Luminescence Spectroscopy. As shown in Table 4, in deoxygenated pure CH_3CN or H_2O/CH_3CN (4:1) solution at 25 °C, the complexes of **1a** (λ_{exc} 480–580 nm) were nonemissive. The $[Ru(tpy)(fctpy)]^{2+}$ and $[Ru(fctpy)_2]^{2+}$ complexes were nonemissive in room-temperature fluid solution.[13] The excited-state lifetime measurements indicated an upper-limit emission lifetime of 25 ns ($\lambda_{max}{}^{em}$ at 600 nm) in 4:1 EtOH/MeOH (v/v) at 77 K, substantially shorter than that found for $Ru(tpy)_2{}^{2+*}$ (τ = 11 μs) at 77 K.[22] The very short lifetime observed for $[Ru(tpy)(fctpy)]^{2+*}$ and $[Ru(fctpy)_2]^{2+*}$ at 77 K has been attributed to the presence of a ferrocenyl moiety, which provides additional channels for excited-state deactivation. The ferrocenyl moiety acts as an efficient quencher for the ^{3}MLCT state.

In our previous report,[12] the insertion of an ethynylene group into the main chain, giving **2a**, causes a dramatic increase in the phosphorescence yield (1.48×10^{-4}), triplet lifetime (67 ns), and emission maximum (690 nm). The binuclear complex **2a** also showed decreased triplet energy in comparison with the mononuclear $[Ru(tpy)(fctpy)]^{2+}$ and $[Ru(fctpy)_2]^{2+}$.[13] Emission in pure acetonitrile was extremely weak. Furthermore, the emission spectra had the same spectral shape, regardless of the excitation wavelength, and differed only in intensity. The increase of radiative activation observed for **2a** relative to **1a** has been attributed to the more pronounced electron delocalization in the extended π^* orbitals. The electron is excited to the ethynylene-substituted tpy ligand, where it is delocalized over the extended π-electron system that includes ferrocenyl subunits. The enhanced luminescence yield and triplet lifetime observed for **2a** relative to **1a** could be explained by the lower lying $^3[Ru^{III}(tpy^-)Fc^{II}]$ MLCT state in **2a** relative to that in **1a**. Because of its lower energy, there will be less pronounced mixing between the $^3[Ru^{III}(tpy^-)Fc^{II}]$ state and the $^3[Ru^{II}(tpy^-)Fc^{III}]$ state. Under these conditions, the ferrocenyl moiety does not acts as an efficient quencher for the $^3[Ru^{III}(tpy^-)Fc^{II}]$ MLCT state.

(23) Mammano, N. J.; Zalkin, A.; Landers, A.; Rheingold, A. L. *Inorg. Chem.* **1977**, *16*, 297–300.

(24) (a) Duggan, D. M.; Hendrickson, D. N. *Inorg. Chem.* **1975**, *14*, 955–970. (b) Hendrickson, D. N.; Sohn, Y. S.; Gray, H. B. *Inorg. Chem.* **1971**, *10*, 1559–1563. (c) Horsfield, A.; Wassermann, A. *J. Chem. Soc. A* **1970**, 3202–3204. (d) Prins, R.; Kortbeek, A. *J. Organomet. Chem.* **1971**, *33*, C33–C34.

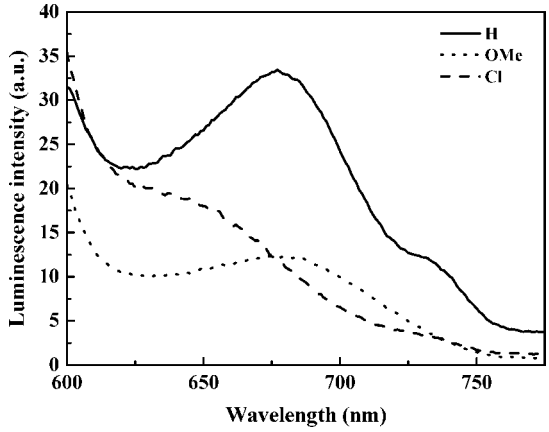

Figure 6. Emission spectra at $\lambda_{exc} = 490$ nm of the indicated complexes in H_2O/CH_3CN (4:1) solution at room temperature.

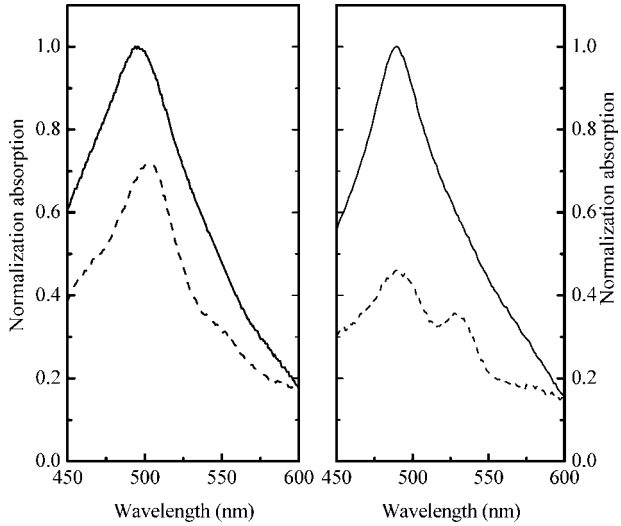

Figure 7. Comparsion of absorption spectra (solid line) in CH_3CN solution and excitation spectra (dashed line, measured at $\lambda_{exc} =$ 647 nm) in H_2O/CH_3CN (4:1) solution for **2b** (left) and **2c** (right).

The attachment of $-OCH_3$ and $-Cl$ substitutents to the terminal tpy in Ru^{2+} complexes of **1b**,**c** to micromodulate the Ru^{2+}/Ru^{3+} and tpy/tpy$^-$/tpy^{2-} redox potentials has no significant influence on the luminescent photophysical properties. Complexes of **1b**,**c** are still nonemissive ($\lambda_{exc} = 480$–580 nm) in deoxygenated pure CH_3CN or H_2O/CH_3CN (4/1) solution at 25 °C. Making a comparison of the electrochemical data of **1b**,**c** with **1a**, we have found that the Fe^{2+}/Fe^{3+} redox potentials for **1b**,**c** are quite similar to those of **1a**. Here, we would like to suggest that the $^3[Ru^{II}(tpy^-)Fc^{III}]$ energy state in **1b**,**c** is not possibly changed by the attachment of $-OCH_3$ and $-Cl$ substitutents. Consequently, the ferrocenyl moiety acts as an efficient quencher.

On comparison of the luminescent properties of **2b**,**c** with those of **2a**, the attachment of $-OCH_3$ and $-Cl$ substitutents causes a decrease of luminescence quantum yields (1.09×10^{-4} for **2b**; 0.45×10^{-4} for **2c**), triplet lifetimes (16 ns for **2b**; 18 ns for **2c**), and emission maxima (696 nm for **2b**; 648 nm for **2c**) (Figure 6 and Table 4). The single emission band indicates that a single excited state is responsible for the emission observed. As shown in Figure 7, a detailed comparison was made between the absorption spectrum and the excitation spectrum. Spectra were plotted with the restriction that the absorption spectrum must be higher in intensity than the excitation spectrum. We noted that the low-energy shoulder assigned to the $^1[(d(\pi)_{Ru})^6] \rightarrow {}^3[d(\pi)^5(\pi^*_{tpy})^1]$ MLCT transition (Ru^{2+}-based MLCT) at ~530 nm was observed in both absorption and excitation spectra of **2b**. In the case of **2c**, it is quite obvious that the $^1[(d(\pi)_{Ru})^6] \rightarrow {}^3[d(\pi)^5(\pi^*_{tpy})^1]$ MLCT band at 527 nm was observed in the excitation spectrum. This is unexpected, since the $^1[(d(\pi)_{Ru})^6] \rightarrow {}^3[d(\pi)^5(\pi^*_{tpy})^1]$ MLCT band was not observed in the excitation spectrum of relevant monomeric $Ru^{2+}-$tpy derivatives.[13,18] In our case, we would like to suggest that it is possible to decay from the higher energy excited state of $^3[d(\pi)^5(\pi^*_{tpy})^1]$ to the lower energy luminescent excited state of $^3[d(\pi)^5(\pi^*_{tpy})^1]$.

When the values of Φ and τ for **2b**,**c** are compared with those for **2a**, we find that **2b**,**c** are weakly emissive. This finding is in line with the electrochemical observations. We have found that the Fe^{2+}/Fe^{3+} redox potentials for **2b**,**c** are more positively shifted in comparison with those of **2a**. The increase of luminescence yields and triplet lifetimes observed for **2b**,**c** relative to **1b**,**c** can be attributed to the more pronounced electron delocalization in the extended π^* orbitals. The electron is excited to the ethynyl-substituted tpy ligand where it is delocalized over the extended π-electron system that includes ferrocenyl subunits. However, the decrease of luminescence yields and triplet lifetimes observed for **2b**,**c** relative to **2a** can possibly be attributed to the lower energy state of $^3[Ru^{II}(tpy^-)Fc^{III}]$ in **2b**,**c**. Under these conditions, the ferrocenyl moiety acts as a more efficient quencher.

Conclusion

Summarizing, we have systematically undertaken electrochemical and photophysical studies to probe the electronic states of **1b**,**c** and **2b**,**c** containing bis(2,2′:6′,2″-terpyridyl)polyferrocene redox-active spacers end capped with photoactive $Ru^{2+}-$terpyridine terminals. The ground-state HOMO and LUMO energies are estimated from electrochemical measurements. To enhance the π-delocalization in the spacer, the oxidation potentials of the ferrocenyl moieties and the tpy reduction potentials are matched as closely as possible by the attachment of $-OCH_3$ and $-Cl$ substitutents. However, a single wave was found for the Ru^{2+}/Ru^{3+} redox couple in the electrochemical measurements of **1b**,**c** and **2b**,**c**, indicating that the electronic coupling between the Ru^{2+} centers is still relatively weak. The attachment of $-OCH_3$ and $-Cl$ substitutents to the terminal tpy in Ru^{2+} complexes of **1b**,**c** has no significant influence on the luminescent photophysical properties. Complexes of **1b**,**c** are still nonemissive in deoxygenated pure CH_3CN or H_2O/CH_3CN (4:1) solution at 25 °C, suggesting that the $^3[Ru^{II}(tpy^-)Fc^{III}]$ energy state in **1b**,**c** is possibly not changed. The decrease of luminescence quantum yields, triplet lifetimes, and emission maxima in **2b**,**c** suggests that the ferrocenyl moiety acts as a more efficient quencher.

Acknowledgment. We thank the National Science Council, Department of Chemistry, and Center for Nanoscience and Nanotechnology at National Sun Yat-Sen University for financial support.

Supporting Information Available: Tables and figures giving complete details of the structural determination of **4**, extracted electrochemical data and cyclic voltammograms with Ag/AgCl as a reference electrode for compounds **1b**,**c** and **2b**,**c**, and spectroscopic data for compounds **1b**,**c** and **2b**,**c**. This material is available free of charge via the Internet at http://pubs.acs.org.

OM700568H